MDP-based Energy-aware Task Scheduling for Battery-less IoT

Shahab Jahanbazi, Mateen Ashraf, Onel L. A. López, Senior Member, IEEE

Abstract—Realizing high long-term task completion rates represents a fundamental challenge in battery-less Internet of Things (IoT) devices powered by ambient energy harvesting. This difficulty is primarily due to the stochastic and timevarying characteristics of the available energy, which significantly complicate the design of optimal task scheduling policies. In this paper, we consider a battery-less IoT device that must periodically report sensing measurements to a monitoring center. We adopt the Markov decision process (MDP) framework to handle energy variability while aiming to maximize the longterm task completion rate. For this, we first identify its components and then define two appropriate reward functions. We demonstrate the inherent properties associated with the MDP formulation and the related optimal policy. Subsequently, we solve the resulting optimization problem, leading to the optimal stationary threshold-based (OSTB) scheduling. Simulation results demonstrate that OSTB outperforms the well-known "as late as possible" (ALAP) scheduling strategy. For instance, an 8.6% increase in the task completion rate, along with a 65% reduction in power failures and a 86.29% decrease in execution delays during task execution are registered assuming a 4.7 mF capacitor.

Index Terms—Battery-less IoT devices, Markov decision process, task scheduling, energy harvesting.

I. INTRODUCTION

NTERNET of Things (IoT) is a rapidly growing network I of interconnected devices that collect and share data, reshaping how people and systems interact with their environment [1]. An active research focus related to these linked devices is the development of battery-less functionality. This feature is supported by relying on ambient energy harvesting (EH) as the charging source, promoting energy sustainability, environmental friendliness, and operational longevity [2]. Nonetheless, one of the most critical challenges is the inevitable intermittent operation, which stems from the variability of energy availability over time [3]-[8]. To mitigate this behavior and ensure sustainable operation, energy-aware protocols are adopted, allowing to dynamically adjust device schedules based on available energy [4], [6]. They are mainly meant for task scheduling [3]-[5], [7]-[9] and/or checkpointing [10], [11] processes.

This work is partially supported in Finland by the Research Council of Finland (Grants 362782 (ECO-LITE), and 369116 (6G Flagship)); and by the European Commission through the Horizon Europe/JU SNS project AMBIENT-6G (Grant 101192113).

The authors are with the Centre for Wireless Communications, University of Oulu, 90014 Oulu, Finland (e-mail: {shahab.jahanbazi; mateen.ashraf; onel.alcarazlopez}@oulu.fi).

Manuscript received April 19, 2021; revised August 16, 2021.

Checkpointing consists of periodically/or adaptively storing system states to maintain forward progress, which however, incurs some energy and time overheads [10]. Meanwhile, task scheduling is the process of allocating atomic tasks to computing resources over time in order to improve energy efficiency. These approaches are often complementary, since task scheduling mitigates the risk of power failure, whereas checkpointing ensures that progress can be preserved and restored across power failure cycles [12]. Note that in batteryless IoT devices that execute collections of atomic tasks, checkpointing is not often necessary and/or affordable. For such systems, where long-running programs are uncommon, and memory and data-processing capabilities are limited, task scheduling is a more suitable and effective strategy. Hereinafter, we focus solely on energy-aware task scheduling approaches, which is a major area of research, that we briefly survey in the following.

Moser et al. [3] introduce a lazy scheduling algorithm, which deliberately defers task execution until their deadlines, reducing premature energy consumption. The approach combines the principles of earliest deadline first and as late as possible (ALAP) scheduling. However, tasks are assumed to consume energy at a constant linear rate, and the scheduler requires an accurate prediction of the harvested energy to function effectively. Meanwhile, varying energy consumption rates for different tasks are considered in [4]-[6], [9]. Sabovic et al. [4] investigate task scheduling for batteryless LoRaWAN devices that perform sensing and transmission in each cycle. They formulate an optimization problem to determine the optimal initial available energy for starting a cycle, aiming to minimize the overall cycle completion time. Moreover, they analyze the trade-offs between keeping the device in sleep mode between tasks and turning it off entirely before the next execution cycle. Sabovic et al. [5] propose an energy-aware task scheduling approach for battery-less IoT devices that accounts for task priorities while modeling dependencies through a single parent-child chain. Carmen et al. [6] extend this idea by considering three independent parent-child chains in addition to incorporating task priorities. Specifically, they formulate the task scheduling problem as a mixed-integer linear program aiming to maximize the number of tasks executed while preventing power failures, and derive an optimal energy-aware algorithm to solve it. Furthermore, to mitigate the computational overhead, the optimization of the proposed objective was confined to a short-term operational window of 15 seconds. All of these works rely on perfect knowledge of future energy arrivals and do not account for

Several studies address the stochastic EH behavior in IoT networks, e.g., [7], [8], [12], [13]. Hao et al. [7] propose a task scheduling approach to sequentially perform sensing and transmission tasks, while aiming to maximize the number of transmission tasks over one day. The formulated problem includes stochastic constraints, which the authors address via equivalent transformations, outputting a framework that is stochastically robust. Kang et al. [12] propose a combined energy-aware task scheduling and checkpointing approach to mitigate power failures. Their work focuses on a setting with a single type of task, where both EH events and task arrivals are modeled as Poisson processes. Rao et al. [8] treat both energy arrival and task arrival as independent stochastic processes in scenarios involving multiple types of tasks. They propose a Markov decision process (MDP)-based framework for optimal task scheduling over a long-term horizon, wherein tasks' deadlines and priorities appear as soft constraints in the utility function. Note that such constraints allow for flexible scheduling when task importance and timing influence but do not strictly dictate execution. However, task deadlines and execution times may be hard constraints in real-time and safety-critical scenarios, as in [14]-[16], calling for more conservative and complex scheduling. For instance, in safetycritical systems, missing a stimulation deadline can result in life-threatening consequences. On the other hand, periodic reporting is necessary in many monitoring applications to ensure that decision-making processes receive timely and fresh updates [17], [18]. In fact, relying only on opportunistic execution may lead to long and unpredictable gaps in reporting, which undermines the reliability and usability of the collected data in real-time applications [19].

To the best of our knowledge, our study here constitutes the first work on task scheduling for battery-less IoT devices that integrates a probabilistic model of harvested energy with the strict enforcement of hard execution time and deadline constraints. The primary contributions of this paper are:

- An optimization problem formulation for long-term task scheduling, and aimed to maximize the task completion rate while simultaneously minimizing the probability of power failures. The formulation explicitly models the trade-off between system reliability and task throughput.
- 2) An MDP-based framework that explicitly incorporates the constraints inherent to the problem. These constraints are embedded within the state and reward definitions, ensuring they are accurately reflected in the decisionmaking process. Moreover, we show that the considered MDP is unichain.
- 3) A novel reward function that explicitly incorporates parameters for handling the frequency of power failures. The function adaptively allocates higher reward values to time slots with greater energy availability, encouraging the execution of tasks during periods of sufficient energy availability. This design enhances the system's robustness against power interruptions and improves overall energy-aware task scheduling performance.
- 4) An optimal stationary threshold-based (OSTB) scheduling strategy based on the defined MDP-based frame-

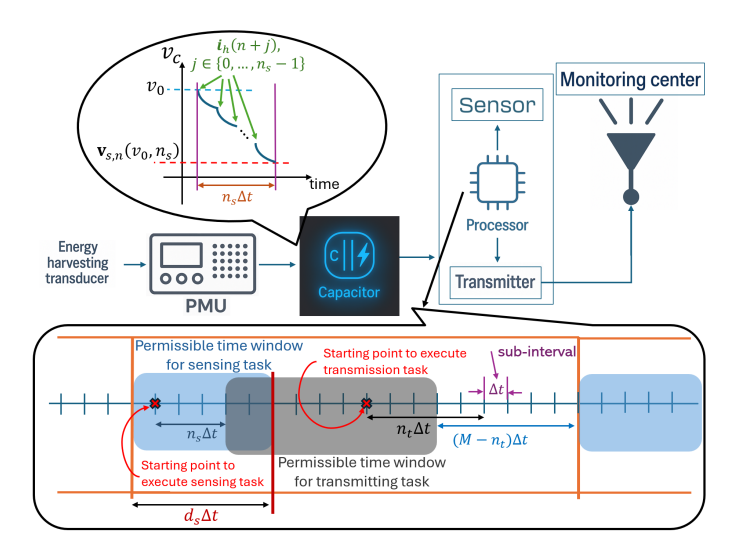


Fig. 1. System model: a battery-less IoT device powered by ambient EH reports sensing measurements to a monitoring center. The concept of permissible time windows for tasks and the changes in voltage across the capacitor during the sensing task are illustrated.

work that maximizes the number of completed tasks over long-term horizon. We rigorously demonstrate that the optimal policy exhibits a threshold-based structure, which considerably reduces the search space and simplifies the optimization process. Moreover, the proposed OSTB scheduling is evaluated against the ALAP approach, demonstrating advantages across multiple criteria, including task completion rate, frequency of power failures, and execution latency.

The remainder of this paper is organized as follows. Section II introduces the system model considered in this study. In Section III, we formulate the problem. Section IV defines the components of the MDP. In Section V, we outline the objective function and discuss the foundational properties of the policy. Moreover, we analyze the characteristics of the optimal policy and derive the resulting optimal scheduling strategy. Section VI presents simulation results that demonstrate the performance of the proposed OSTB scheduling and ALAP algorithm. Finally, our conclusions are provided in Section VII.

II. SYSTEM MODEL

As shown in Fig. 1, this paper considers a battery-less IoT device powered by an ambient energy source. The device's EH module includes a transducer, a power management unit (PMU), and a capacitor that stores the harvested energy. The latter is consumed by a load consisting of a microprocessor, a sensor, and a wireless transmitter.

The device operates in a periodic cycle of T_s seconds. At the beginning of each cycle, the device tries to initiate a sensing task during which a target/environment parameter is measured. This can be postponed, though, until a predefined deadline d_s in case of insufficient energy resources. Once sensing is completed, the measured data is transmitted to the monitoring center. Transmission must be fully completed within the ongoing cycle, i.e., before the beginning of the

next cycle, when a new sensing task may be executed. Consequently, within every cycle interval, the device performs exactly one sensing operation followed by one data transmission. For analytical purposes, each cycle is further divided into M equal subintervals of length $\Delta t = T_s/M$ (cf. Fig. 1). This subdivision enables a finer-grained characterization of the system's behavior and facilitates the evaluation of its performance within each cycle. Following this, the durations of the sensing and transmission operations are n_s and n_t basic scheduling units, respectively.

Although the sensing period determines when new measurements are expected, practical systems rarely guarantee that the task starts exactly at the nominal instant due to scheduling delays, sensor wake-up latencies, or communication contention. For this reason, we introduce a deadline that defines the latest permissible start time of the sensing task within each period, thereby ensuring that the acquired data remains valid and fresh. Note that bounding the start-time window is essential for maintaining freshness and timely performance in wireless IoT systems [20], [21]. Following this, within each cycle, the sensing task may commence at any time up to a specified deadline of d_s units.

To handle the execution process, we define a permissible time window for each task. It is defined as the set of time units during which the execution can be started. As depicted in Fig. 1, the permissible time window for the sensing task comprises the set $\mathcal{PTW}^{(s)} = \{0, \cdots, d_s\}$ to reflect the deadline constraint. Moreover, the set for the transmitting task would be $\mathcal{PTW}^{(t)} = \{n_s, \cdots, M - n_t\}$ to reflect that the transmitting can only be performed after executing the sensing task and before reaching the end of the current main interval. Indeed, $\mathcal{PTW}^{(t)}$ starts from n_s because the earliest opportunity to execute the transmission task occurs immediately after the commencement of the sensing task at the beginning of the main interval, which requires n_s time units. According to the proposed mechanism, the sensing task can be interpreted as a high-priority task compared to the transmission task.

The device may also sleep with a one-sub-interval duration and fixed energy consumption during idle periods. This basic fine-grained low-power mode inclusion ensures that no potential operational scenario is overlooked. In particular, when the available energy in a sub-interval is inadequate to perform any task, modeling sleep allows the system to wait for the next opportunity to initiate execution.

We assume that the harvested current during the n-th subinterval, denoted by $\mathbf{i}_h(n)$, is constant throughout the considered sub-interval and is assumed to be i.i.d. across the subintervals. Moreover, the connected load behaves as a constant resistance [2], [4], [6] for each mode. Specifically, each mode is modeled by a load resistance $R_i = \frac{E}{I_i}$, where E is the operating voltage and I_i denotes the current drawn in mode $i \in \{l, s, t\}$. During both sleep and task execution modes, the available energy in the capacitor undergoes variation due to discharging or charging (cf. Fig. 1). Assuming that the initial

voltage across the capacitor at the start of the n-th sub-interval is v_0 , and the device enters a certain mode i for n_i sequential sub-intervals, the resulting capacitor voltage is given by

$$\mathbf{v}_{i,n}(v_0, n_i) = e^{-\frac{n_i \Delta t}{R_i C}} \times \left(v_0 + R_i (1 - e^{-\frac{\Delta t}{R_i C}}) \sum_{j=0}^{n_i - 1} \mathbf{i}_h(n+j) e^{(j+1)\frac{\Delta t}{R_i C}} \right). \tag{1}$$

Note that for the special case of $n_l = 1$, this transforms into the well known $e^{-\frac{\Delta t}{R_l C}}(v_0 + R_l(1 - e^{-\frac{\Delta t}{R_l C}})\mathbf{i}_h(n)e^{\frac{\Delta t}{R_l C}})$.

One key phenomenon constraint that affects the decision-making process is the potential occurrence of a power failure. More specifically, the device cannot complete the execution of the ongoing task if the capacitor voltage drops below the turn-off threshold V_{out} . Due to this, we introduce *safety probability* metric for the execution of task i, which is defined as

$$P_{\text{safe}}^{(i)}(v_0) = \mathbb{P}(\mathbf{v}_{i,n}(v_0, n_i) \ge V_{\text{out}}), \quad \forall i \in \{s, t\}. \tag{2}$$

It is worth noting that, since the harvested current is assumed to be i.i.d., this parameter is independent of n, and therefore we drop this from the notation of $P_{\rm safe}^{(i)}(v_0)$. Moreover, n_i is omitted, since the task identifier itself encodes the execution time, which is given as a prefix. The device must execute task i within $\mathcal{PTW}^{(i)}$, during which the safety probability is high. Therefore, to enable optimal task scheduling, it is essential to develop a framework that comprehensively captures all the aforementioned restrictions and constraints.

III. PROBLEM FORMULATION

We focus on maximizing the long-term average number of tasks successfully executed. To formalize this, let $z_k^{(i)}$ and $v_{z_k^{(i)}}$ denote the starting time unit and its corresponding voltage to execute task $i \in \{s,t\}$ during the k-th main interval, respectively. Formally,

$$z_k^{(s)} \in \mathcal{PTW}^{(s)},\tag{3}$$

$$z_k^{(t)} = z_k^{(s)} + n_s + q_k \in \mathcal{PTW}^{(t)},$$
 (4)

where $q_k \in \mathcal{Q}_k = \{0, \cdots, M - n_t - (z_k^{(s)} + n_s)\}$ to imply that the transmission task can only be initiated q_k time units after the completion of the sensing task, which itself requires n_s time units to execute. Let us define the task completion indicator as

$$\xi_k^{(i)} = \mathbb{1}\{\exists z_k^{(i)}: P_{\text{safe}}^{(i)}(v_{z_s^{(i)}}) \geq 1 - \epsilon\}, \forall i \in \{s, t\}, \quad \text{(5)}$$

where $\mathbb{1}\{.\}$ denotes the indicator function and ϵ is the maximum tolerable risk threshold.

Let $v_{k,0}$ denotes the capacitor voltage at the beginning of the k-th main interval, then using $\xi_{k-1}^{(i)}$ we can write $v_{k,0}$ in the recursive form shown in (6). Note that once the final possible task has been executed, the device will remain in sleep mode for the remainder of the interval. For the first case in (6), if neither the sensing task nor the transmitting task is executed during the previous main interval, the device remains in sleep mode throughout that interval. For the second case in (6), if only the sensing task is executed, then the device enters sleep

¹The notations $i=l,\,i=s,$ and i=t correspond to the sleeping, sensing, and transmitting modes, respectively.

$$v_{k,0} = \begin{cases} \mathbf{v}_{l,0}(v_{k-1,0}, M), & \xi_{k-1}^{(s)} = \xi_{k-1}^{(t)} = 0, \\ \mathbf{v}_{l,z_{k-1}^{(s)} + n_s}(\mathbf{v}_{s,z_{k-1}^{(s)}}(v_{z_{k-1}^{(s)}}, n_s), M - z_{k-1}^{(s)} - n_s), & \xi_{k-1}^{(s)} = 1, \xi_{k-1}^{(t)} = 0, \\ \mathbf{v}_{l,z_{k-1}^{(t)} + n_t}(\mathbf{v}_{t,z_{k-1}^{(t)}}(v_{z_{k-1}^{(t)}}, n_t), M - z_{k-1}^{(t)} - n_t), & \xi_{k-1}^{(s)} = \xi_{k-1}^{(t)} = 1. \end{cases}$$

$$(6)$$

mode once the task is completed and stays in that mode until the end of the interval (i.e., from $z_{k-1}^{(s)}$ to the (M-1)-th time unit). Likewise, if the transmitting task is executed, as in the third case in (6), the device transitions to sleep mode immediately after completing the task and remains in that state for the remainder of the interval.

The voltage at time unit $z_k^{(s)}$ depends on $v_{k,0}$ as

$$v_{z_k^{(s)}} = \begin{cases} v_{k,0}, & z_k^{(s)} = 0, \\ \mathbf{v}_{l,0}(v_{k,0}, z_k^{(s)}), & z_k^{(s)} \in \mathcal{PTW}^{(s)} \setminus 0, \end{cases}$$
(7)

where the second case corresponds to the final voltage after the device has remained in sleep mode for $z_k^{(s)}$ units. Following this, the capacitor voltage at time unit $z_k^{(t)}$ to start performing the transmitting task within the k-th main interval can be written as

$$v_{z_{k}^{(t)}} = \begin{cases} \mathbf{v}_{s,z_{k}^{(s)}}(v_{z_{k}^{(s)}}, n_{s}), & q_{k} = 0, \\ \mathbf{v}_{l,z_{k}^{(s)} + n_{s}}(\mathbf{v}_{s,z_{k}^{(s)}}(v_{z_{k}^{(s)}}, n_{s}), q_{k}), & q_{k} \in \mathcal{Q}_{k} \setminus 0, \end{cases}$$
(8)

where the first case $q_k=0$, represents the capacitor voltage immediately after completing the sensing task, while the second case corresponds to the voltage after the device has remained in sleep mode for q_k time units following the sensing operation.

The optimization problem is formulated as

$$\begin{array}{ll}
\text{maximize} & \lim_{K \to \infty} \frac{1}{K} \sum_{k=1}^{K} \xi_k^{(s)} (1 + \xi_k^{(t)}) \\
\{z_k^{(s)}, z_k^{(t)}\} & K \to \infty
\end{array} \tag{9a}$$

subject to
$$v_{z_k^{(i)}} \in [V_{min}, V_{max}], \quad \forall i \in \{s,t\}, k \in \mathbb{N}, \ \mbox{(9b)}$$

$$(3), (4), (5), (6), (7), (8),$$
 (9c)

where V_{min} and V_{max} correspond to the minimum and maximum permissible operating voltages, respectively. Note that (9a) accounts for the fact that the execution of a transmitting task is feasible only if the corresponding sensing task has been completed beforehand within the designated main interval. Since (9) involves stochastic constraints and its objective function is defined over a long-term time horizon, directly tackling this problem is not straightforward. To address this, we reformulate it in the next section as an MDP, which offers a structured framework for modeling long-term sequential decision-making under uncertainty. Indeed, we incorporate the aforementioned constraints into the MDP components' design and leverage the framework to facilitate the search for an effective solution and to derive the values of $\{v_{z_k^{(s)}}, v_{z_k^{(t)}}\}_{k \in \mathbb{N}}$ systematically.

IV. MDP DESIGN

In this section, we first define the key components of the MDP-based approach. We then introduce two transition matrices, which together allow for a more tractable analytical representation. Finally, we present two distinct reward functions that form the basis of the proposed objective function.

A. State Space

Since the execution time for sensing and transmitting tasks comprises several sub-intervals, we define an epoch in the MDP framework as a single decision stage, corresponding to one transition in the state space (i.e., observation of the current state, action selection, and transition to the next state). At the n-th epoch, the state of the system is captured by a three-element vector s_n as

$$s_n = (V_n, \tau_n, f_n), \tag{10}$$

where $V_n \in [V_{min}, V_{max}]$ denotes the capacitor voltage, $\tau_n \in \{0, \cdots, M-1\}$, referred to as the *local clock*, represents the index of the sub-interval within the main interval, and $f_n \in \{0,1,2\}$, termed as the *task flag*, indicates whether a sensing or transmitting tasks have already been executed in the current main interval. Specifically, we have $f_n = 0$ if the sensing task is executable, $f_n = 1$ if the sensing has already occurred in the current main interval, and $f_n = 2$ if the transmission has already been performed in the current main interval.

As the voltage variable V_n is continuous, the associated state space is infinite. To enable the application of classical finitestate MDP methods and to facilitate the evaluation of longterm performance criteria, we quantize the V_n onto N_v levels, i.e., $V_n \in \mathcal{V} \triangleq \{V^{(1)}, V^{(2)}, \cdots, V^{(N_v)}\}$, where $V^{(1)} = V_{min}$ and $V^{(N_v)} = V_{max}$. The two state elements τ_n and f_n track the process within the main interval and determine whether the allowable task is still executable. Specifically, the sensing task can only be carried out if $\tau_n \in \mathcal{PTW}^{(s)}$ and $f_n = 0$, while the transmission task is allowed if $\tau_n \in \mathcal{PTW}^{(t)}$ and $f_n = 1$. At the beginning of each main interval, both the task flag and the local clock are reset to $\tau_n = f_n = 0$. Taking these considerations into account, and after applying the quantization operation, the set of all admissible system states forms the state space S, which contains a finite number of elements, denoted by N_s .

With the above state space design, the next state of the process depends solely on the current state and the action taken in that state, rather than the entire history of past states and actions. This property clearly indicates that the problem adheres to the non-memory Markov property, which is fundamental in MDPs.

B. Action Space

The action space in the considered system is defined as

$$A = \{\text{sleeping, sensing, transmitting}\}.$$
 (11)

5

At the beginning of each sub-interval, the agent evaluates its current state, and then selects an action a from the set of allowable actions in that state. This set for state $s=(V,\tau,f)$, denoted by \mathcal{A}_s , remains constant over time and is defined as

$$\mathcal{A}_s = \begin{cases} \{\text{sleeping, sensing}\}, & s \in \mathcal{S}_1, \\ \{\text{sleeping, transmitting}\}, & s \in \mathcal{S}_2, \\ \{\text{sleeping}\}, & s \in \mathcal{S} \setminus \{\mathcal{S}_1, \mathcal{S}_2\}, \end{cases}$$

where S_1 denotes the set of all states with $\tau \in \mathcal{PTW}^{(s)}$ and f = 0, and S_2 represents all the states with $\tau \in \mathcal{PTW}^{(t)}$ and f = 1.

C. State Transition Probability Matrix

The state transition probability matrix encapsulates the probabilistic dynamics of the system and defines how the state of the system evolves as a result of the actions taken by the agent. Note that the simplifying assumption of treating the harvested current as an i.i.d. process across sub-intervals leads to a transition matrix that remains invariant with respect to the process's evolution. For ease of readability, we initially consider the deterministic part of the state (i.e., τ and f) and obtain N_v states for each possible pair, and denote it as superstate (τ, f) . More formally, the collection of states corresponding to the fixed parameters τ and f is referred to as a superstate (τ, f) , including N_v states as $(V, \tau, f), \forall V \in \mathcal{V}$.

We define two levels of transition matrices to model the system dynamics: micro transition matrices, which capture transitions for individual actions, and a macro transition matrix, which integrates these micro transition matrices across the entire state space.

- 1) Micro Transition Matrices: The transitions between voltage levels, occurring as the system evolves from one superstate to another, are governed by a set of action-dependent transition matrices. Each of these matrices is of size $N_v \times N_v$ and encodes the probabilities of transitioning between discrete voltage levels under a specific action. As there are three possible actions, we define three micro transition matrices, denoted by A_l , A_s , and A_t , which correspond respectively to the sleeping, sensing, and transmitting actions.
- 2) Macro Transition Matrix: The macro transition matrix is a global matrix of size $N_s \times N_s$, constructed from the micro transition matrices A_l , A_s , A_t , and the zero matrix $\mathbf{0}_{N_v \times N_v}$. It encodes the all transitions between all possible superstates in the system. Specifically, the matrix has the following properties:
 - Sensing action: For superstate $(\tau, f = 0)$, where $\tau \in \mathcal{PTW}^{(s)}$, the next superstate is $(\tau + n_s, f = 1)$ which is governed by A_s .
 - Transmitting action: For superstates $(\tau, f = 1)$, where $\tau \in \mathcal{PTW}^{(t)}$:
 - if $\tau < M n_t$, the next superstate is $(\tau + n_t, f = 2)$,
 - if $\tau = M n_t$, the next superstate is (0,0). which this transition is governed by A_t .
 - Sleeping action: Governed by A_l , which advances the system by one sub-interval. For superstates (τ, f) where:

$$-0 \le \tau < M-1, f=0,$$

-
$$n_s \le \tau < M - 1$$
, $f = 1$,
- $n_s + n_t \le \tau < M - 1$, $f = 2$,
the next superstate is $(\tau + 1, f)$.

- Interval reset: At the end of the main interval, the system resets the local clock and task flag. For superstates $(\tau = M 1, f \in \{0, 1, 2\})$, the next superstate is (0, 0), with transition governed by A_l .
- Invalid transitions: For all other superstate pairs not covered above, the transition matrix is defined as $\mathbf{0}_{N_v \times N_v}$, indicating that transitions are not permitted.
- 3) Example: Here, we provide an example to illustrate the above concepts. Without loss of generality, we assume that the device can take only two actions: sleeping and sensing. However, the discussion in the example can be naturally extended to include transmitting action as well.

Consider a periodic approach in which the sensing task is executed once every $T_s = 1$ second. Moreover, every onesecond interval is divided into M=8 equal sub-intervals. The sensing task is characterized by two parameters: a deadline of $d_s = 3$ sub-interval units, and an execution time of $n_s = 3$ units. The voltage quantization grid is defined with $N_v = 3$ discrete levels. As shown in Fig. 2 (left), to satisfy the deadline constraint, the agent for each state within the first four superstates with $(\tau \in \{0,1,2,3\}, f = 0)$ can choose sleeping or sensing. These choices are closely tied to the selected policy, which is discussed in detail in Section V. More specifically, the system can transition from state $(V^{(i)}, \tau, 0)$ where $\tau \leq 3$ to state $(V^{(j)}, \tau + n_s, 1)$ with probability $A_s(i, j)$, provided the agent selects sensing action. Alternatively, if the agent chooses sleeping action while in state $(V^{(i)}, \tau, f)$, where $f \in \{0, 1\}$, the system will move to state $(V^{(j)}, \tau + 1, f)$ for $\tau < M - 1$ and to state $(V^{(j)}, 0, 0)$ for $\tau = M - 1$ with probability $A_l(i, j)$.

Furthermore, in Fig. 2 (right), the overall structure of the macro transition matrix is depicted, capturing all possible actions that may lead from one state to another. Note that the action selected by the agent, as determined by the policy, is reflected only in the first four rows of the transition matrix, corresponding to the superstates $(\tau \in \{0,1,2,3\}, f=0)$. For states belonging to the remaining superstates, the only permissible action is sleeping; consequently, this action is identical across all policies.

D. Reward Function

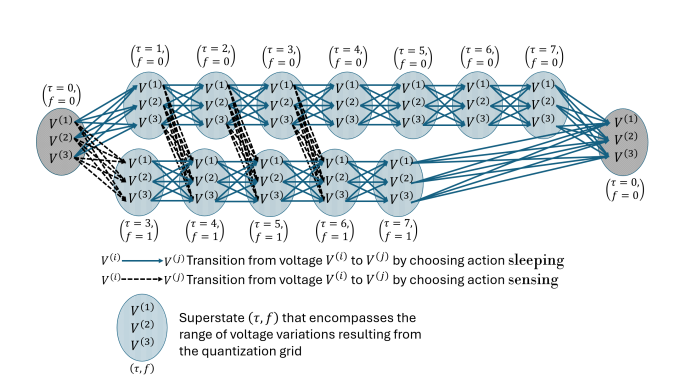
We design two reward functions tailored to reflect the system's operational efficiency, thereby ensuring that only safe actions contribute to the agent's performance in each state. They capture the reward received by the agent upon taking action a_n in state $s_n = (V_n, \tau_n, f_n)$.

1) Basic Reward Function: This reward function is primarily defined in terms of the safety probability as

$$r(s_n \in \mathcal{S}_1, a_n = \text{sensing}) = P_{\text{safe}}^{(s)}(V_n),$$

 $r(s_n \in \mathcal{S}_2, a_n = \text{transmitting}) = P_{\text{safe}}^{(t)}(V_n),$
 $r(s_n \in \mathcal{S}, a_n = \text{sleeping}) = 0.$ (13)

Recall that the safety probability $P_{safe}^{(i)}(V_n), \forall i \in \{s,t\}$ is defined in (2), and the sets \mathcal{S}_1 and \mathcal{S}_2 are defined in Section



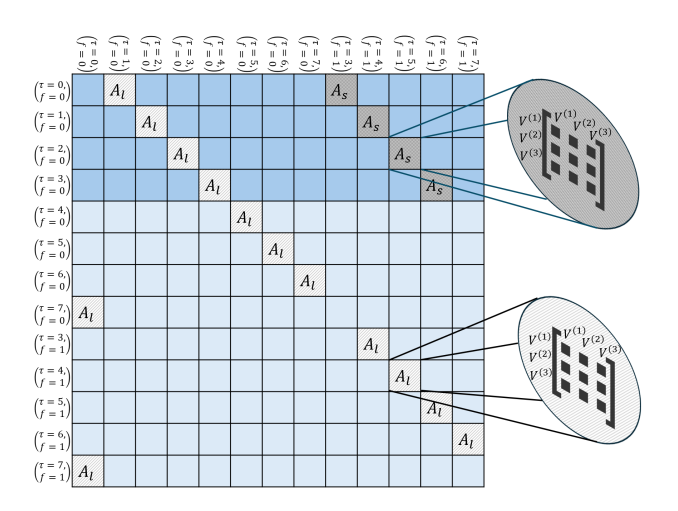


Fig. 2. An illustrative representation of the scheme described in Section IV-C3, assuming M=8, $N_v=3$, $d_s=3$, and $n_s=3$. Fig. 2 (left) shows the forward progress of the process, including the defined superstates. Fig. 2 (right) presents the general form of the transition matrix, where all possible action choices are considered. Each part in this matrix corresponds to a sub-matrix associated with a specific action that leads to a transition to another state in a different superstate. In particular, for rows corresponding to superstates with $(\tau \in \{0,1,2,3\}, f=1)$, the policy selects the appropriate rows from either A_l or A_s , depending on the action taken.

IV-B. This function assigns higher rewards to states with higher voltage levels, thereby encouraging the agent to actively engage in task execution when sufficient energy is available. Moreover, it is a non-decreasing and monotonic function with respect to the initial voltage (i.e., V_n), which can reduce the complexity of the MDP formulation [22] as further discussed in Section V-C.

2) Sigmoid-based Reward Function: This reward function includes additional parameters to provide greater control over power failure. Specifically, we use a normalized sigmoid function, characterized by a steepness parameter β and threshold value θ as

$$\begin{split} r(s_n \in \mathcal{S}_1, a_n = \text{sensing}) &= \frac{1 + e^{-\beta(P_{\text{safe}}^{(s)}(V_{max}) - \theta)}}{1 + e^{-\beta(P_{\text{safe}}^{(s)}(V_n) - \theta)}}, \\ r(s_n \in \mathcal{S}_2, a_n = \text{transmitting}) &= \frac{1 + e^{-\beta(P_{\text{safe}}^{(s)}(V_{max}) - \theta)}}{1 + e^{-\beta(P_{\text{safe}}^{(t)}(V_n) - \theta)}}, \\ r(s_n \in \mathcal{S}, a_n = \text{sleeping}) &= 0. \end{split} \tag{14}$$

It should be noted that the parameter θ serves a restrictive role by effectively enforcing the scheduling of task i whenever the value of $P_{\rm safe}^{(i)}(V_n)$ exceeds θ . This mechanism effectively reduces the occurrence of power failures. More specifically, as illustrated in Fig. 3, the reward values defined in (13) corresponding to states with moderate voltage levels are disregarded according to (14). Consequently, states associated with higher voltage levels are prioritized in the scheduling process, ultimately leading to a reduction in power failures.

V. OPTIMAL POLICY

Herein, we first introduce the considered objective function, followed by the policy types in our MDP. In addition, we establish the unichainity property of the problem under consideration, and then show that the optimal policy has a threshold-based structure. Finally, we determine the optimal policy that maximizes the long-term average reward.

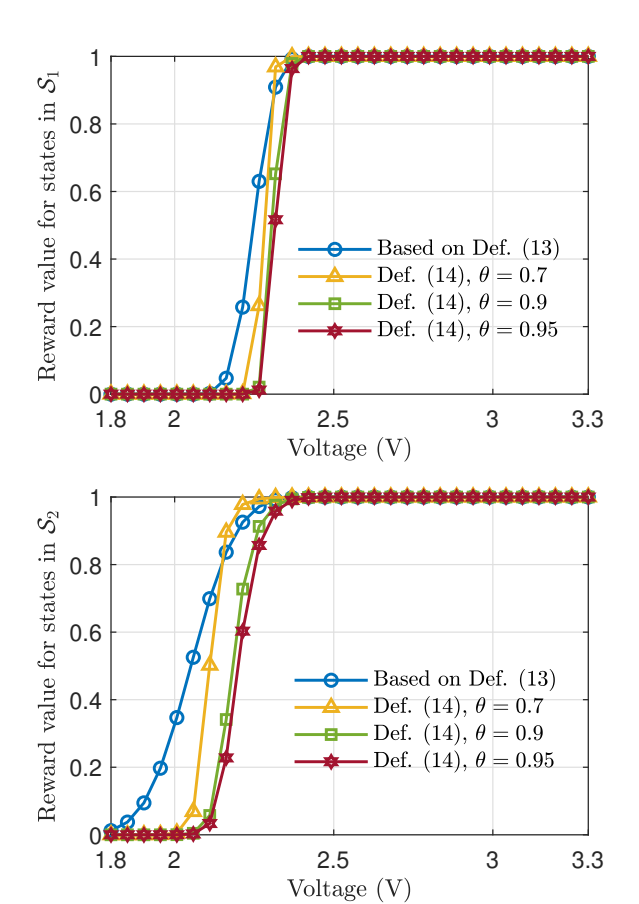


Fig. 3. Reward values from (13) and (14) with $\beta=15$ and $\theta\in0.7,0.9,0.95$ as functions of voltage for states in \mathcal{S}_1 with action sensing (top) and states in \mathcal{S}_2 with action transmitting (bottom), with C=2.7mF, $V_{out}=2.4\text{V}$, and \mathbf{i}_b has an i.i.d. uniform distribution as $\mathcal{U}[0,3]\text{mA}$.

A. Objective Function

The objective is to develop a scheduling policy that effectively utilizes the available energy to maximize the task completion rate over a long-term horizon while minimizing the risk of power failure. To formally capture this objective, we adopt the long-term average reward criterion, a standard metric in MDP-based formulations. In this framework, the policy $\pi: \mathcal{S} \to \mathcal{A}_s$ is defined as a mapping from each state to its allowable action set. Let $s_0 = s$ indicate the initial system state, then the average expected reward of a policy π , denoted by $g^{\pi}(s)$, is defined as

$$g^{\pi}(s) = \lim_{N \to \infty} \frac{1}{N} \left[\sum_{n=0}^{N-1} r^{\pi}(s_n, a_n) | s_0 = s \right], \quad (15)$$

where $r^{\pi}(s_n, a_n)$ denotes the reward received at the *n*-th epoch upon taking action a_n in state s_n under policy π . Then, the aim is to find an optimal policy π^* that maximizes the average expected reward across all admissible policies as

$$\pi^* = \arg\max_{\pi} g^{\pi}(s), \forall s \in \mathcal{S}. \tag{16}$$

Given that the average expected reward function is defined as a limit and depends on the initial state, determining the optimal policy requires a deeper understanding of its structure.

B. Policy Types and Unichainity Property

Policies in MDPs can be described along two dimensions: deterministic versus stochastic, and stationary versus non-stationary. Among these, deterministic and stationary policies are of particular importance, as they often serve as natural candidates for both theoretical analysis and practical implementation. Here, we examine these two properties in detail within the framework of the proposed MDP, highlighting their role in shaping decision-making across states and over time.

Deterministic Policy: A policy is said to be deterministic if, for each state $s \in \mathcal{S}$, it selects a single action with certainty [22]. One common deterministic policy is thresholdbased decision-making. For example, in the proposed MDP in superstates including states where sensing is permitted (i.e., $s \in \mathcal{S}_1$), the policy may choose the sensing action if the safety probability satisfies $P_{safe}(V) \geq \gamma$, and choose sleeping otherwise. Here, γ is a fixed threshold parameter that may depend on the second component of the state (e.g., τ). For instance, in Section IV-C3, a possible deterministic policy may be defined as follows. In the superstate $(\tau = 2, f = 0)$, the policy selects the action sleeping for all states of the form (V, τ, f) , where $V \in \{V^{(1)}, V^{(2)}\}$, and selects the action sensing for the state $(V^{(3)}, \tau, f)$. In contrast, within the superstate $(\tau = 3, f = 0)$, the policy assigns the action sleeping to state where $V^{(1)}$, and the action sensing to states with $V \in \{V^{(2)}, V^{(3)}\}.$

Stationary Policy: A policy is stationary if it remains unchanged over time and depends only on the current state, not explicitly on the time index or decision step [22], [23]. For example, in Section IV-C3, whenever the process occupies a state of the form $s = (V, \tau, f)$ whit $\tau \in \{0, 1, 2, 3\}$ and f = 0, the agent applies the same transition rule to determine the subsequent state.

Certain structural properties of the Markov chains (MCs) induced by policies can be exploited for analyzing MDPs

with long-term average reward criteria to find the optimal policy. Specifically, for any deterministic stationary policy π , the induced MC partitions the state space into one or more irreducible recurrent classes, along with a possible set of transient states [24]. Moreover, according to [22, Proposition 8.2.1], any two states within the same closed, irreducible recurrent class share the same average expected reward g^{π} . Consequently, if the MC induced by every deterministic stationary policy contains exactly one recurrent class (possibly with transient states), known as the unichain property, then $g^{\pi}(s)$ is the same for all states s. This ensures the optimality criterion is independent of the initial state and is robust across the entire state space.

Theorem 1. Let π be an arbitrary stationary deterministic policy. Moreover, let the transition matrices A_l , A_s , and A_t be time-invariant and have strictly positive elements. Then, the MC induced by π contains exactly one recurrent class (possibly along with a set of transient states).

Proof. The proof is provided in Appendix A.

C. Threshold-based property of the optimal policy

The complexity of finding the optimal policy in an MDP stems from the size of the state and action spaces, as the search for the optimal policy must be conducted over their joint space. Even without reducing the number of state-action pairs, the complexity of solving an MDP can be mitigated by designing a well-structured reward function that guides the policy toward simpler, more efficient forms, such as threshold-based decisions [8]. This property enables efficient computation to obtain the optimal policy by limiting the policy search to only those policies that have the threshold-based structure [22].

For clarification, a threshold-based policy within our MDP refers to a decision rule in which, at each sub-interval within the permissible time window, the device chooses to execute the corresponding task only if the voltage across the capacitor exceeds a specified threshold. Before presenting the formal theorem implying this property, we provide an interpretation of the necessity of the constraints required to hold as a remark in the following.

Remark 1. The policy iteration algorithm uses a Bellmantype equation for the long-term average reward criterion, where the Q-function is defined as $Q(s,a) = r(s,a) + \sum_{s'} P(s'|s,a)h(s')$. During policy improvement, the algorithm greedily selects actions that maximize this Q-function, ultimately converging to an optimal policy. Following this, we define a function named action advantage function, which quantifies the advantage of taking action sensing over sleeping at state $(V^{(i)}, m, 0)$ where $m \in \mathcal{PTW}^{(s)}$ as

$$\Delta(V^{(i)}, m) = Q((V^{(i)}, m, 0), sensing) - Q((V^{(i)}, m, 0), sleeping)$$

$$= r((V^{(i)}, m, 0), sensing) + \sum_{j} A_{s}(i, j)h(V^{(j)}, m + n_{s}, 1)$$

$$- \sum_{j} A_{l}(i, j)h(V^{(j)}, m + 1, 0), \qquad (17)$$

where we apply $r((V^{(i)},m,0),s \texttt{leeping}) = 0$, following the definition of reward functions in Section IV-D. We aim to prove that $\Delta(V^{(i)},m)$ is non-decreasing in $V^{(i)}$. This would imply the existence of a threshold V_m^* such that the optimal action is s leeping for $V^{(i)} < V_m^*$ and s ensing for $V^{(i)} \ge V_m^*$, establishing the threshold structure. Since $\Delta(V^{(i)},m)$ is determined by the reward and transition matrices, proving the threshold-based property necessitates certain regularity conditions on these elements. Specifically, we make use of the conditions stated in [22, Th. 8.11.3], and the following theorem demonstrates that these conditions are satisfied within our framework.

Theorem 2. Under the definition of MDP and both reward functions provided in Section IV, there exists an optimal deterministic stationary policy π^* that is threshold-based in V within each superstate. That is, for superstates $(\tau = m, f = 0)$, where $m \in \mathcal{PTW}^{(s)}$, there exist threshold parameters $\{V_m^*\}_{m=0}^{d_s}$ such that

$$\pi^*((V, m, 0)) = \begin{cases} \text{sleeping, if } V < V_m^*, \\ \text{sensing, if } V \ge V_m^*. \end{cases}$$
 (18)

And for superstates $(\tau = m, f = 1)$, where $m \in \mathcal{PTW}^{(t)}$, there exist threshold parameters $\{W_m^*\}_{m=n_s}^{M-n_t}$ such that

$$\pi^*((V, m, 1)) = \begin{cases} \text{sleeping,} & \text{if } V < W_m^*, \\ \text{transmitting,} & \text{if } V \ge W_m^*. \end{cases}$$
 (19)

Proof. The proof is provided in Appendix B

Remark 2. About stationary property within our defined MDP, a possible question arises: if the policy threshold γ is a function of τ_n , does that make the policy non-stationary? The answer is no, as long as the policy depends only on the current state $s_n = (V_n, \tau_n, f_n)$, and not on the absolute time step n. The apparent time-dependence through τ_n is absorbed into the state definition, and thus the policy remains a fixed mapping from states to actions and unchanged over time.

For unichain MDPs, the maximum long-term average reward and the corresponding optimal stationary policy can be computed using well-established methods, such as linear programming approaches [22], [23]. Herein, we utilize the following linear program from [23, eq. 10] to derive the optimal policy.

$$\begin{aligned} & \underset{x(s,a)}{\text{maximize}} & & \sum_{s \in \mathcal{S}} \sum_{a \in \mathcal{A}_s} x(s,a) r(s,a) \\ & \text{s.t.} & & x(s,a) \geq 0, \quad \forall s \in \mathcal{S}, a \in \mathcal{A}_s, \\ & & \sum_{s \in \mathcal{S}} \sum_{a \in \mathcal{A}_s} x(s,a) = 1, \\ & & \sum_{a \in \mathcal{A}_{s'}} x(s',a) = \sum_{s \in \mathcal{S}} \sum_{a \in \mathcal{A}_s} x(s,a) P(s'|s,a), \forall s' \in \mathcal{S}, \end{aligned}$$

We employ the CVX package in MATLAB to solve the linear programming formulation, which enables us to compute the optimal stationary distribution $x^*(s,a)$ associated with the given MDP. According to [22, Corollary 8.8.3], in any state

TABLE I PARAMETERS FOR THE CONSIDERED PROBLEM

Description	Symbol	Value		
Turn-off threshold	V_{out}	1.8 V		
Capacitance	C	4.7 mF		
Minimum Operating Voltage	V_{min}	1.8 V		
Maximum Operating Voltage	V_{max}	3.3 V		
Duration of Each Sub-interval	Δt	0.02 s		
Deadline for executing sensing task	$d_s \Delta t$	0.3 s		
Number of sub-intervals	M	50		
Current Consumption of Sleep	I_l	0.1 mA		
Current Consumption of Sensing task	I_s	1.7 mA		
Current Consumption of Transmitting task	I_t	4.36 mA		
Number of Levels for Descritization	N_v	30		
Execution Time of Sensing Task	$n_s \Delta t$	0.1 s		
Execution Time of Transmitting Task	$n_t \Delta t$	$\{0.4, 0.8\}$ s		

 $s \in \{S_1, S_2\}$ where tow different actions are admissible, the resulting optimal policy prescribes selecting the action $a \in A_s$ for which $x^*(s, a) > 0$. This procedure directly determines the structure of the optimal scheduling strategy.

VI. SIMULATION RESULTS

In this section, we provide and discuss simulation results. Unless stated otherwise, we adopt the parameter values listed in Table I. We divide our discussions into two parts. The first part focuses on results from using the proposed MDP-based scheme, while the second one provides a comparison with respect to task completion rate, latency, and power failure occurrence numbers between the proposed OSTB scheduling and ALAP algorithm [3].

Following a similar approach to prior studies on EH systems (e.g., [25], [26]), the harvested current is modeled as an i.i.d. uniform process as $\mathbf{i}_h \sim \mathcal{U}[0,3]$ mA. Furthermore, it is assumed that the system is required to execute tasks periodically every $T_s=1$ second.

A. Performance of the OSTB scheduling approach

Fig. 4 (top) illustrates the long-term average expected reward with respect to the execution time of the "sensing" task. Here, the execution time of the "transmitting" task is fixed to 0.8 seconds for three different values of θ . As the execution time of the "sensing" task increases, the objective function exhibits a decreasing trend. This behavior is due to the reduced likelihood of being able to schedule and execute the "transmitting" task within the permissible time window, thereby lowering the overall expected reward. Meanwhile, Fig. 4 (bottom) shows the average expected reward with respect to the "transmitting" task's execution time while the execution time of the "sensing" task is fixed at 0.1 seconds. Similar to the previous case, the average expected reward decreases as the execution time of the transmitting task increases. This reduction occurs because longer transmission durations constrain the opportunity of successfully executing it within the remaining portion of the main interval. Notably, most of the objective function values lie between 1 and 2. This range indicates that, on average, between one and two tasks are executed successfully per main interval, reflecting contributions

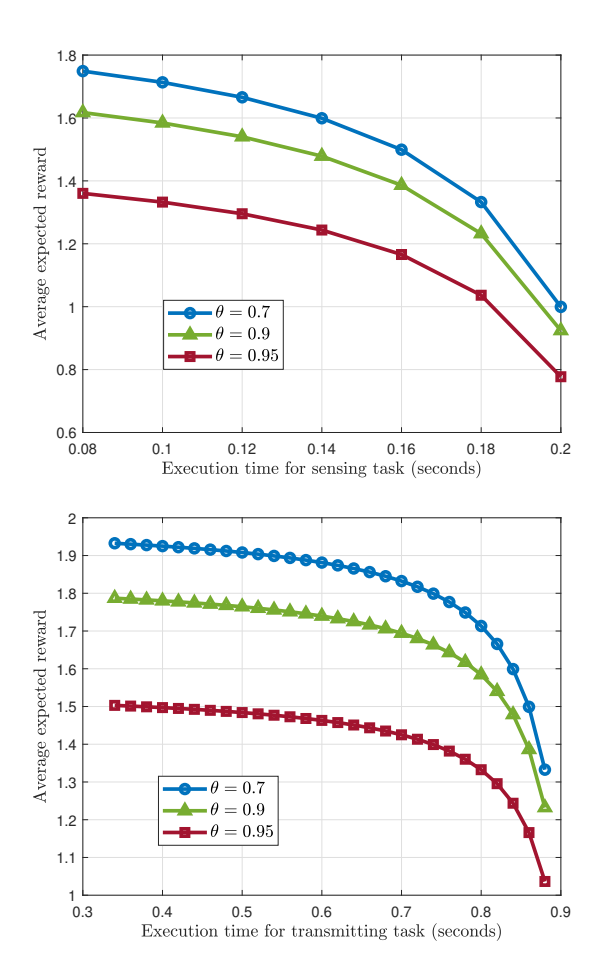


Fig. 4. The average expected reward defined in equation (15) versus the execution times of sensing, while the execution time for transmitting task set $n_t \Delta t = 0.8 \text{ s}$ (top) and versus the execution times of transmitting, while the execution time for sensing task set $n_s \Delta t = 0.1 \text{ s}$ (bottom). For this analysis, the reward function is specified with $\beta = 25$, and the parameter θ is considered at three levels: 0.7, 0.9, and 0.95.

from both "sensing" and "transmitting" executions. In general, Fig. 4 illustrates that the objective function is non-increasing and concave-like with respect to the execution time duration of tasks. For instance, in Fig. 4 (top), as the sensing execution time $n_s\Delta t$ increases, the reduction in the average expected reward becomes more significant. This implies that the impact of increasing execution time is not linear: small increments in n_s at lower values (e.g., from 0.10 to 0.12 seconds) result in relatively minor changes in the objective, whereas the same increment at higher values (e.g., from 0.18 to 0.20 seconds) leads to a more substantial drop.

By solving the linear programming problem mentioned in Section V, we can find the resulting optimal policy. The dependence of optimal threshold voltages with respect to subintervals within $\mathcal{PTW}^{(s)}$ and $\mathcal{PTW}^{(t)}$ on capacitance and distribution of the harvested current is depicted in Fig. 5. Note that the scheduler adopts a conservative strategy in case of low energy availability at the beginning of each main interval, opting to delay task execution in favor of harvesting energy to ensure safer task execution. However, as the end of the permissible time window for each task approaches and the risk

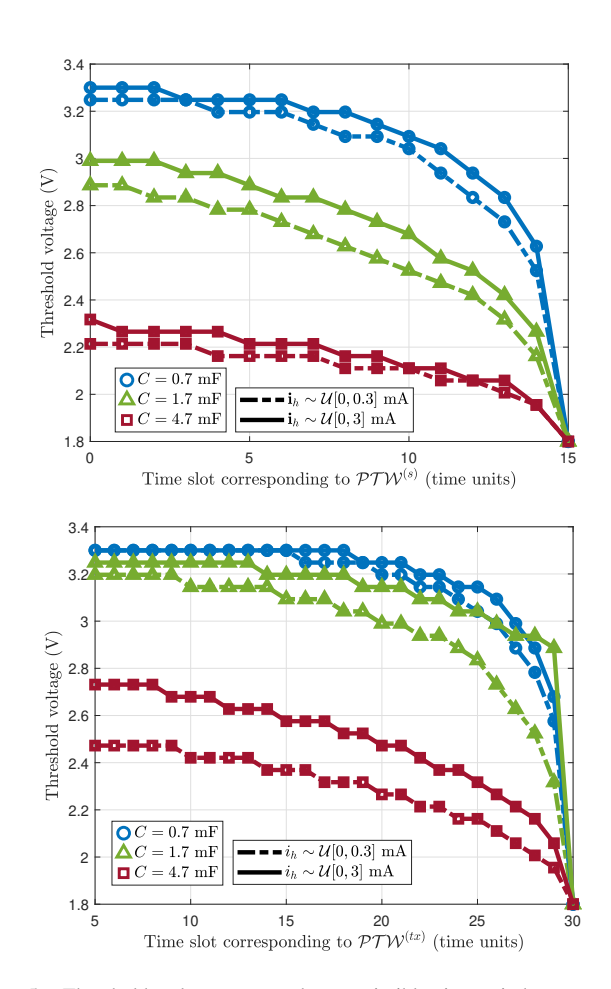


Fig. 5. Threshold voltage versus the permissible time window to execute sensing (top) and to execute transmitting (bottom), for $d_s=15$, $n_s=5$, $n_t=20$, and two distinct uniform distributions for the harvested current as $\mathcal{U}[0,0.3]$ mA and $\mathcal{U}[0,3]$ mA.

of missing the task increases, the scheduler gradually lowers its threshold for acceptable rewards and chooses to execute lower-reward actions even in states with limited available energy. Although the likelihood of reaching these states is negligible when the harvested current is distributed as $\mathbf{i}_h \sim \mathcal{U}[0,9]$ mA, as discussed later. This conservative behavior is generally aligned with the lazy scheduling algorithm [3]. Moreover, the simulation results in Fig. 5 support the conclusion of Theorem 2, since a threshold-based policy yields the maximum average expected reward resulting from solving the mentioned problem.

Simulation results indicate that the threshold voltage during $\mathcal{PTW}^{(s)}$ is lower than that observed during $\mathcal{PTW}^{(t)}$. This behavior is attributed to the "transmitting" task's longer execution duration and higher current consumption. Hence, the scheduler needs to follow a more conservative strategy during the "transmitting" task. Moreover, increasing the range of harvested current leads to an increase in the threshold voltage levels for task execution. This is because a higher harvested current increases the likelihood of successfully executing tasks within their allowable time window. In contrast, the scheduling policy adopts a more conservative approach by selecting higher threshold voltage levels. These elevated thresholds enhance the

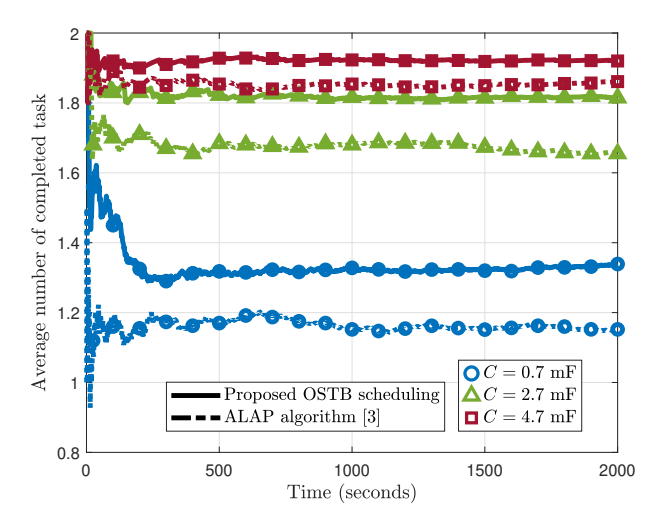


Fig. 6. Average number of completed tasks per time unit for three various values of C. The harvested current is assumed to be $\mathbf{i}_h \sim \mathcal{U}[0,3]$ mA.

probability of safe task execution, which in turn contributes to a higher task completion rate.

B. OSTB vs ALAP

To compare the resulting OSTB scheduling strategy, we consider ALAP algorithm, which schedules tasks toward the end of their allowable time windows [3]. We deliberately chose ALAP as the benchmark for two reasons. First, the problem considered in this work assumes that only two tasks are executed sequentially within T_s -length time slots, where task execution times are relatively smaller than T_s . This constraint makes many recent heuristics for heterogeneous or multiprocessor environments inapplicable without substantial modification, whereas ALAP can be directly applied. Second, by postponing tasks until their deadlines, ALAP intuitively reduces the likelihood of power failures, making it a reasonable baseline for reliability. However, our approach not only achieves fewer power failures but also improves the task completion rate, demonstrating clear structural advantages. Thus, while more advanced benchmarks exist, ALAP remains a meaningful baseline in this context, and our results show clear improvements over it.

Fig. 6 depicts the task completion rate per main interval over time, obtained using the Monte Carlo method. Note that OSTB consistently achieves a higher rate of successful task execution, while ALAP allows more time for EH, which in turn increases energy availability and supports safer task execution. However, within the constraints of the considered system model, deferring task execution until the latest permissible moment can reduce the likelihood of timely completion. This limitation stems from the stochastic EH nature, where delaying the "sensing" task until its deadline may leave insufficient time or energy to complete the subsequent "transmitting" task within the remaining interval. This effect ultimately lowers the overall task completion rate. Moreover, it is important to note that the difference in rate of completed tasks between ALAP and OSTB becomes less pronounced when a larger capacitor is

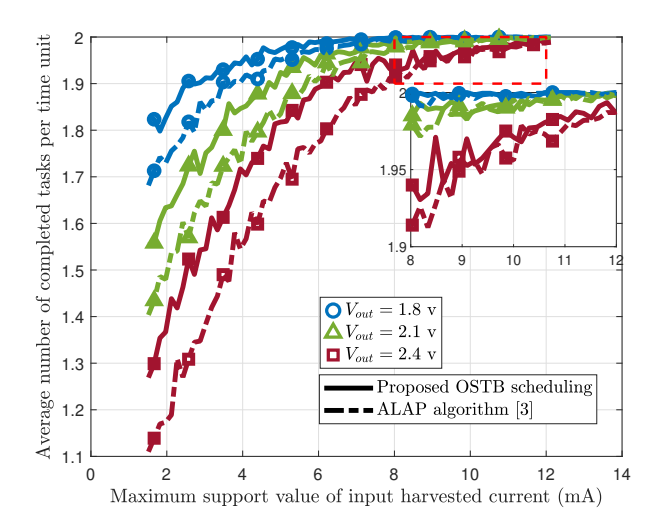


Fig. 7. Average number of completed tasks per time unit versus different values of the support set of the harvested current for three various values of V_{out} over 2000-second duration.

used. In this case, the voltage variation across the capacitor is more stable. Since the average directly depends on the capacitor voltage, the resulting average number also exhibits more stable behavior.

Fig. 7 illustrates the task completion rate over a 2000second duration for various V_{out} and different maximum values of the harvested current, modeled as $\mathbf{i}_h \sim \mathcal{U}[0, \gamma]$. The results indicate that when the turn-off threshold V_{out} is set to 1.8V, the minimum γ required to achieve the maximum task completion rate (i.e., successful execution of both tasks within each main interval) is 7.3mA. In contrast, for higher threshold voltages of 2.1V and 2.4V, the corresponding minimum γ values increase to 11.2mA and exceed 12mA, respectively. Furthermore, it is shown that the task completion rates of both OSTB and ALAP approaches converge for higher values of γ . This observation implies that, as the harvested current increases, deferring task execution until the latest permissible time becomes a viable strategy, particularly in scenarios where execution delay is not a critical concern. These results illustrate the fact that the performance improvement is more pronounced when the support range of harvesting current (i.e., γ) is small. This makes OSTB particularly suitable for ultra-low-power IoT devices.

Table II captures the number of power failures observed for different values of the harvested current simulated for 2000 seconds. It appears that power failures occur more frequently during the execution of the "transmitting" task compared to the "sensing" task. This trend is due to the longer execution time and higher energy consumption associated with "transmitting" task. Moreover, OSTB implementation leads to a decrease in the frequency of power failures.

Another key metric to consider is the latency in task execution. It might seem preferable for the "sensing" task to start at the beginning of each 1-second time interval, followed by the "transmitting" task as soon as possible. However, this ideal execution sequence may be delayed in order to avoid power failures. To account for this delay, we consider the latency in

Value of harvested current	$\mathbf{i}_h \sim \mathcal{U}[0,3]$ mA				$\mathbf{i}_h \sim \mathcal{U}[0,6]$ mA				$\mathbf{i}_h \sim \mathcal{U}[0,9]$ mA			
Task	sens	sing	g transmitting		sensing transm		itting sen		sing transmitting		nitting	
Approach	OSTB	ALAP	OSTB	ALAP	OSTB	ALAP	OSTB	ALAP	OSTB	ALAP	OSTB	ALAP
Number of power failure	37	95	107	162	3	14	11	26	0	2	1	5

TABLE II

COMPARISON OF THE NUMBER OF POWER FAILURES FOR DIFFERENT HARVESTED CURRENT VALUES

TABLE III
TASK EXECUTION LATENCY (UNITS OF TIME)

Value of harvested current	$\mathbf{i}_h \sim \mathcal{U}[0,3] \; \mathrm{mA}$		$\mathbf{i}_h \sim \mathcal{U}[0]$	0, 6] mA	$\mathbf{i}_h \sim \mathcal{U}[0,9] \; \mathrm{mA}$		
Approach	OSTB	ALAP	OSTB	ALAP	OSTB	ALAP	
Overall Latency (s)	163.46	921.36	135.54	988.74	114.38	999.28	

task execution, which refers to the time difference between the desired execution time and the actual time at which the task is performed. Table III presents the overall latency in task execution for both approaches over a 2000-second duration. In this analysis, time intervals affected by power failures are excluded. Note that for OSTB, increasing the range of harvested current leads to a reduction in execution latency. This occurs because the higher energy availability allows tasks to be executed more promptly. In contrast, although ALAP also benefits from fewer power failures at higher harvested current levels, it includes a larger number of 1-second intervals in the delay calculation. Consequently, due to the inherent nature ALAP (i.e., its tendency to defer task execution as late as possible), the overall execution latency increases.

VII. CONCLUSION AND FUTURE DIRECTION

This paper addressed the existing on-off intermittent behavior of battery-less IoT devices. We considered the harvested energy as a stochastic process and focused on the task scheduling approach for a device that executes only two tasks periodically. We proposed an MDP-based framework to determine an optimal task scheduling approach, named OSTB. For this, we defined the components of the MDP that carefully reflect our original problem in this framework. They incorporate constraints on deadline and priority in the definition of the state space, while the constraint on safety execution is taken into account in the design of the reward function. Furthermore, we formulated the objective (i.e., the task completion rate) as an optimization problem based on the long-term average reward criterion. To solve this optimization problem by utilizing well-known methods, we proved the unichainity of the considered MDP. Simulation results clearly showed the effectiveness of the OSTB policy in task execution, demonstrating a higher task completion rate compared to ALAP. Furthermore, the proposed OSTB strategy results in lower values for both power failure and latency, indicating improved efficiency during task execution.

APPENDIX A PROOF OF THEOREM 1

We first introduce a higher-level representation of the chain for simplicity. Given deterministic stationary policy π , define the *policy-induced superstate-level graph* $G_{\pi} = (R, E_{\pi})$, where

- the vertex set R consists of all superstates (τ, f) ; and
- there is a directed edge $S \to T$ if, under π , some state in $S = (\tau_1, f_1)$ has positive probability of transitioning to $T = (\tau_2, f_2)$ in one step at the superstate level.

Because the micro transition matrices A_l , A_s , and A_t have strictly positive entries, the following holds. If $S \to T$ in G_π , then there exists at least one state in S that has positive probability of reaching *every* N_v -component of T in one superstate-level step. Thus, studying reachability and recurrence at the superstate-level is valid for the full state-level chain.

Tail superstates: We define the tail superstates as

$$(\tau, f = 0), \quad \tau \in \{d_s + 1, \dots, M - 1\},$$

$$(\tau, f = 1), \quad \tau \in \{M - n_t + 1, \dots, M - 1\},$$

$$(\tau, f = 2), \quad \tau \in \{n_s + n_t, \dots, M - 1\}.$$

In these superstates, the only allowable action is sleeping, which deterministically advances τ by +1 without changing f until reaching M-1, at which point the process wraps to (0,0).

Reachability of (0,0): From any initial state $(V^{(i)},\tau,f)$, the chain reaches some tail superstate under any π . Once in a tail superstate, repeatedly chosen sleeping action advances τ until $\tau=M-1$ and then moves to (0,0). Therefore, (0,0) is reachable from every state in the chain with strictly positive probability.

Possible disconnections in G_{π} and transience: Two cases may lead to transient states:

- 1) Disconnection at $(\tau_0, f = 0) \to (\tau_0 + 1, f = 0)$, for $\tau_0 \in \mathcal{PTW}^{(s)}$. This can occur if the agent chooses sensing for all states in $(\tau_0, f = 0)$. In this case, all subsequent tail superstates $(\tau, f = 0)$ with $\tau > \tau_0$ become transient.
- 2) Disconnection at $(\tau_1, f = 1) \rightarrow (\tau_1 + 1, f = 1)$, for $\tau_1 \in \mathcal{PTW}^{(t)}$. This can occur if the agent chooses

transmitting for all states in $(\tau_1, f=1)$. In this case, all subsequent tail superstates $(\tau, f=1)$ with $\tau > \tau_1$ are transient.

Existence of exactly one recurrent class: Despite these possible transient sets, note that

- every state in the chain has a positive-probability path to (0,0) (reachability);
- once in (0,0), the positivity of the micro transition matrices ensures communication between all N_v -components in every superstate reachable from (0,0);
- any recurrent class must contain (0,0), because (0,0) is reachable from every state and recurrent classes are closed.

Since there can be at most one recurrent class containing (0,0), the MDP is unichain.

APPENDIX B PROOF OF THEOREM 2

To establish the threshold-based property of the optimal policy with respect to the state variable V, we use [22, Th. 8.11.3]. This theorem provides the necessary conditions for the structure of rewards and transitions, namely monotonicity and superadditivity to prove the existence of the optimal threshold-based policy. To show that these conditions are met in our considered problem, we fix a superstate $(\tau=m,f=0), \forall m\in \mathcal{PTW}^{(s)}$ and analyze the structure of the optimal policy.

From the definition of the reward function in (13) or (14), we observe that r((V,m,0),a) is non-decreasing in V when $a=\mathtt{sensing}$. For all other state-action pairs, the reward is zero, thereby trivially satisfying the monotonicity condition. Furthermore, this property implies that

$$r((V', m, 0), a') + r((V, m, 0), a) \ge r((V', m, 0), a) + r((V, m, 0), a')$$

for V'>V and a= sleeping and a'= sensing and then r((V,m,0),a) is superadditive in (V,a). Furthermore, the transition matrices A_l and A_s govern the evolution of V under the actions sleeping and sensing, respectively. These matrices are stochastically monotone. Specifically, increasing V causes the distribution over future values of V to shift stochastically to the right. This property satisfies the superadditivity condition. Having verified the structural assumptions of [22, Th. 8.11.3], we conclude that the optimal stationary policy π^* under the long-term average reward criterion exhibits a threshold-based structure in V. The proof for superstates $(m,f=1)_{n_s}^{M-n_t}$ is the same. \square

REFERENCES

- [1] O. L. A. López, O. M. Rosabal, D. E. Ruiz-Guirola, P. Raghuwanshi, K. Mikhaylov, L. Lovén, and S. Iyer, "Energy-sustainable IoT connectivity: Vision, technological enablers, challenges, and future directions," *IEEE Open Journal of the Communications Society*, vol. 4, pp. 2609– 2666, 2023.
- [2] O. L. A. López, M. Ashraf, S. Nasser, G. M. de Jesus, R. K. Singh, M. C. Filippou, and J. Famaey, "Foundations for energy-aware zero-energy devices: From energy sensing to adaptive protocols," 2025. [Online]. Available: https://arxiv.org/abs/2507.22740

- [3] C. Moser, D. Brunelli, L. Thiele, and L. Benini, "Real-time scheduling for energy harvesting sensor nodes," *Real-Time Syst.*, vol. 37, no. 3, p. 233–260, Dec. 2007.
- [4] A. Sabovic, C. Delgado, D. Subotic, B. Jooris, E. De Poorter, and J. Famaey, "Energy-aware sensing on battery-less LoRaWAN devices with energy harvesting," *Electronics*, vol. 9, no. 6, 2020. [Online]. Available: https://www.mdpi.com/2079-9292/9/6/904
- [5] A. Sabovic, A. K. Sultania, C. Delgado, L. D. Roeck, and J. Famaey, "An energy-aware task scheduler for energy-harvesting batteryless IoT devices," *IEEE Internet of Things Journal*, vol. 9, no. 22, pp. 23 097– 23 114, 2022.
- [6] C. Delgado and J. Famaey, "Optimal Energy-Aware Task Scheduling for Batteryless IoT Devices," *IEEE Transactions on Emerging Topics in Computing*, vol. 10, no. 3, pp. 1374–1387, 2022.
- [7] J. Hao, J. Chen, R. Wang, Y. Zhuang, and B. Zhang, "A Robust Transmission Scheduling Approach for Internet of Things Sensing Service with Energy Harvesting," Sensors, vol. 19, no. 14, 2019.
- [8] V. S. Rao, R. V. Prasad, and I. G. M. M. Niemegeers, "Optimal task scheduling policy in energy harvesting wireless sensor networks," in 2015 IEEE Wireless Communications and Networking Conference (WCNC), 2015, pp. 1030–1035.
- [9] C. Delgado, J. M. Sanz, C. Blondia, and J. Famaey, "Batteryless LoRaWAN communications using energy harvesting: Modeling and characterization," *IEEE Internet of Things Journal*, vol. 8, no. 4, pp. 2694–2711, 2021.
- [10] M. Hicks, "Clank: Architectural support for intermittent computation," in 2017 ACM/IEEE 44th Annual International Symposium on Computer Architecture (ISCA), 2017, pp. 228–240.
- [11] P. Singla, S. S. Singh, and S. R. Sarangi, "Flexicheck: An adaptive checkpointing architecture for energy harvesting devices," in 2019 Design, Automation & Test in Europe Conference & Exhibition (DATE), 2019, pp. 546–551.
- [12] Y.-m. Kang and Y.-s. Lim, "Handling power depletion in energy harvesting iot devices," *Electronics*, vol. 13, no. 14, 2024.
- [13] A. Biason, S. Dey, and M. Zorzi, "A decentralized optimization framework for energy harvesting devices," *IEEE Transactions on Mobile Computing*, vol. 17, no. 11, pp. 2483–2496, 2018.
- [14] M. Karimi, H. Choi, Y. Wang, Y. Xiang, and H. Kim, "Real-time task scheduling on intermittently powered batteryless devices," *IEEE Internet* of Things Journal, vol. 8, no. 17, pp. 13 328–13 342, 2021.
- [15] R. M. Pathan, "Fault-tolerant and real-time scheduling for mixed-criticality systems," *Real-Time Syst.*, vol. 50, no. 4, p. 509–547, Jul. 2014. [Online]. Available: https://doi.org/10.1007/s11241-014-9202-z
- [16] F. M. S. Nascimento and G. Lima, "Effectively scheduling hard and soft real-time tasks on multiprocessors," in 2021 IEEE 27th Real-Time and Embedded Technology and Applications Symposium (RTAS), 2021, pp. 210–222.
- [17] E. Aerabi, M. Fazeli, and D. Hély, "Cyense: Cyclic energy-aware scheduling for energy-harvested embedded systems," *Microprocessors* and *Microsystems*, vol. 89, p. 104421, 2022. [Online]. Available: https://www.sciencedirect.com/science/article/pii/S0141933121005597
- [18] M. Chetto and R. El Osta, "Earliest deadline first scheduling for real-time computing in sustainable sensors," *Sustainability*, vol. 15, no. 5, 2023. [Online]. Available: https://www.mdpi.com/2071-1050/15/5/3972
- [19] Z. Yuan, Y. Ge, J. Wei, S. Yuan, R. Liu, and X. Mo, "Energy prediction for energy-harvesting wireless sensor: A systematic mapping study," *Electronics*, vol. 12, no. 20, 2023. [Online]. Available: https://www.mdpi.com/2079-9292/12/20/4304
- [20] B.-S. Kim, "A priority-aware dynamic scheduling algorithm for ensuring data freshness in 5g networks," Future Generation Computer Systems, vol. 163, p. 107542, 2025. [Online]. Available: https://www.sciencedirect.com/science/article/pii/S0167739X24005065
- [21] N. Lu, B. Ji, and B. Li, "Age-based scheduling: Improving data freshness for wireless real-time traffic," ser. Mobihoc '18. New York, NY, USA: Association for Computing Machinery, 2018, p. 191–200. [Online]. Available: https://doi.org/10.1145/3209582.3209602
- [22] M. L. Puterman, Markov Decision Processes: Discrete Stochastic Dynamic Programming, 2nd ed. US: Wiley, 2005.
- [23] P. Sakulkar and B. Krishnamachari, "Online Learning Schemes for Power Allocation in Energy Harvesting Communications," *IEEE Trans*actions on Information Theory, vol. 64, no. 6, pp. 4610–4628, 2018.
- [24] S. M. Ross, Introduction to Stochastic Dynamic Programming. CA USA: Academic, 1983.
- [25] R. V. Prasad, V. S. Rao, C. Sarkar, and I. Niemegeers, "ReNEW: A Practical Module for Reliable Routing in Networks of Energy-Harvesting Wireless Sensors," *IEEE Transactions on Green Communications and Networking*, vol. 5, no. 3, pp. 1558–1569, 2021.

[26] M. Gorlatova, A. Wallwater, and G. Zussman, "Networking low-power energy harvesting devices: Measurements and algorithms," *IEEE Transactions on Mobile Computing*, vol. 12, no. 9, pp. 1853–1865, 2013.